

SUPPORTING INFORMATION

Growth of Manganese Oxide Nanostructures Alters the Layout of Adhesion on a Carbonate Substrate

Chongzheng Na and Scot T. Martin

School of Engineering and Applied Sciences & Department of Earth and Planetary Sciences,
Harvard University, Cambridge, MA 02138

May 10, 2009

Total number of pages: 11

Number of Tables: 3

Table S1. Chemistry of 1-mM experimental solution

Table S2. Piecewise linear regression of $f_{adh}(\text{MnO}_x)$ and pH for the data shown in Figure 3

Table S3. *t*-Test on the regressions of $f_{adh}(\text{MnCO}_3)$ with pH

Number of Figures: 7

Figure S1. Experimental setup for the measurement of force-distance curves

Figure S2. Raw data corresponding to the force-distance curves shown in Figure 1

Figure S3. Linear regression of the transition data in Figure 1b

Figure S4. Uncertainty in the AFM tip radius

Figure S5. A representative force-distance curve showing that electrostatic repulsion dominates over van-der-Waals attraction

Figure S6. Three sets of representative force curves.

Figure S7. One set of topography and adhesion images at pH 9.5.

Table S1. Chemistry of 1-mM Experimental Solution

No.	1	2	3	4	5	6	7	8
NaNO ₃ added (mM)	0.99	0.999	0.9999	0.999	0.995	0.99	0.98	0.9
HNO ₃ added (mM)	0.01	0.001	0.0001					
NaOH added (mM)				0.001	0.005	0.01	0.02	0.1
Calculated pH	5.0	6.0	6.8	8.0	8.7	9.0	9.3	10
Measured pH	4.97	6.05	6.5	7.09	7.94	8.59	9.06	9.73
Total Dissolved CO ₂ (mM) [†]	0.02	0	0.0003	0.006	0.02	0.001	0.004	0.007
P _{CO₂} (atm) [†]	7×10 ⁻⁴	0	4×10 ⁻⁶	9×10 ⁻⁷	2×10 ⁻⁷	5×10 ⁻⁶	3×10 ⁻⁶	4×10 ⁻⁷

[†] The lowering of pH from its calculated value arises from the dissolution of carbon dioxide in the solution. The most abundant species of dissolved CO₂ is bicarbonate in the range of our experimental pH. Bicarbonate concentration was calculated using Visual MINTEQ 2.51 (<http://www.lwr.kth.se/English/OurSoftware/vminteq>).

Table S2. Piecewise Linear Regression of $f_{adh}(\text{MnO}_x)$ and pH for the Data Shown in Figure 3[†]

Variable	Value						
pH	5.0	6.0	6.5	7.1	7.9	8.6	9.7
Reconstructed pH ₁	5.0	6.0	6.5	7.1	7.1	7.1	7.1
Reconstructed pH ₂	0	0	0	0	0.8	1.5	2.6
$\log f_{adh}(\text{MnO}_x)$ (pN)	2.22	2.15	2.41	2.84	2.67	2.46	2.44

Source	Degrees of Freedom	Sum of Squares [‡]	Mean Square	<i>F</i> Value	Probability > <i>F</i>
Model [§] : $f_{max} = apH_1 + bpH_2 + c$	2	0.1116	0.0558	0.96	0.3
Residual Error	4	0.2334	0.0584		
Total Error	6	0.3450			

Parameter	Degrees of Freedom	Estimate	Standard Error	<i>t</i> Value	Probability > $ t $
<i>a</i>	1	0.29	0.10	2.9	0.02
<i>b</i>	1	-0.10	0.08	1.25	0.16
<i>c</i>	1	0.64	0.63	1.01	0.21

[†] F-test and *t*-test follow standard procedures outlined in *Introduction to the Practice of Statistics* by Moore and McCabe, W. H. Freeman and Company, New York, 1998.

[‡] $R^2 = 3052/3184 = 0.96$ and adjusted $R^2 = 0.95$.

[§] Equation 3 is obtained by converting this model back to two linear models, one for $\text{pH} < 7.1$ and the other for $\text{pH} \geq 7.1$, using estimated values of *a*, *b*, and *c*.

Table S3. *t*-Test on the Regressions of $f_{adh}(\text{MnCO}_3)$ with pH[†]

Dependent Variable	Parameter	Degrees of Freedom	Estimate	Standard Error	<i>t</i> Value	Probability > $ t $ [*]
$f_{adh}(\text{MnCO}_3)$	slope	5	19	13	1.5	0.19
	Intercept	5	0.023	0.116	0.2	0.85

[†] *t*-test follows standard procedures outlined in *Introduction to the Practice of Statistics* by Moore and McCabe, W. H. Freeman and Company, New York, 1998

^{*} Large probabilities indicate that there is no linear relation between $f_{adh}(\text{MnCO}_3)$ and u .

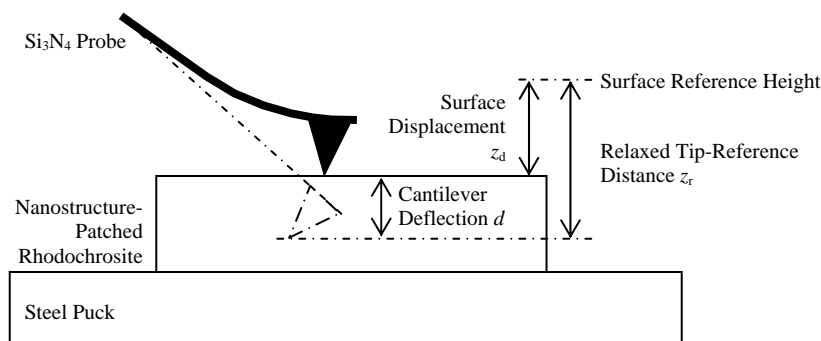


Figure S1. Experimental setup for the measurement of force-distance curves. The components above the steel puck are immersed in solution. Drawing is not to scale, and the cantilever deflection is greatly exaggerated. The force measurement is conducted as follows. The surface starts at a reference height in contact with the tip of the probe. Their contact is ensured by having the cantilever of the probe bent to a preset amount of 15 – 30 nm under contact pressure. Cantilever deflection d is measured by a laser beam shone on the back of the probe cantilever, which reflects the laser light onto a photodiode detector. The photodiode detector gives a reading in voltage V , which is proportionally related to d through cantilever sensitivity s and its baseline value V_0 : $d = s(V - V_0)$. The distance between the relaxed position of the probe tip (i.e., as if the tip did not experience any interfacial force and thus the probe cantilever did not bend) and the reference height is z_r . From the reference height, the sample stage gradually descends until the tip is separated from the surface in small steps of a few nanometers or less. At each step, the microscope records the displacement z_d of the surface. Before the tip is separated from the surface, we have $z_d + d - z_r = 0$. We can thus readily estimate the cantilever sensitivity by the linear regression of z_d with V because $z_d = z_r - s(V - V_0)$ and z_r and V_0 are constants. After the tip and the surface are separated, their distance z is $z_d - z_r - d$ (note: $z = 0$ when the tip and the surface are in contact). Cantilever deflection d can be further converted to the interfacial force that the probe experiences using Hook's law: $f = kd$, where k is the cantilever spring constant and estimated *a priori*. In summary, the measurement at one sampling location gives a V - z_d plot of the experimental data that can be further converted to an f - z plot.

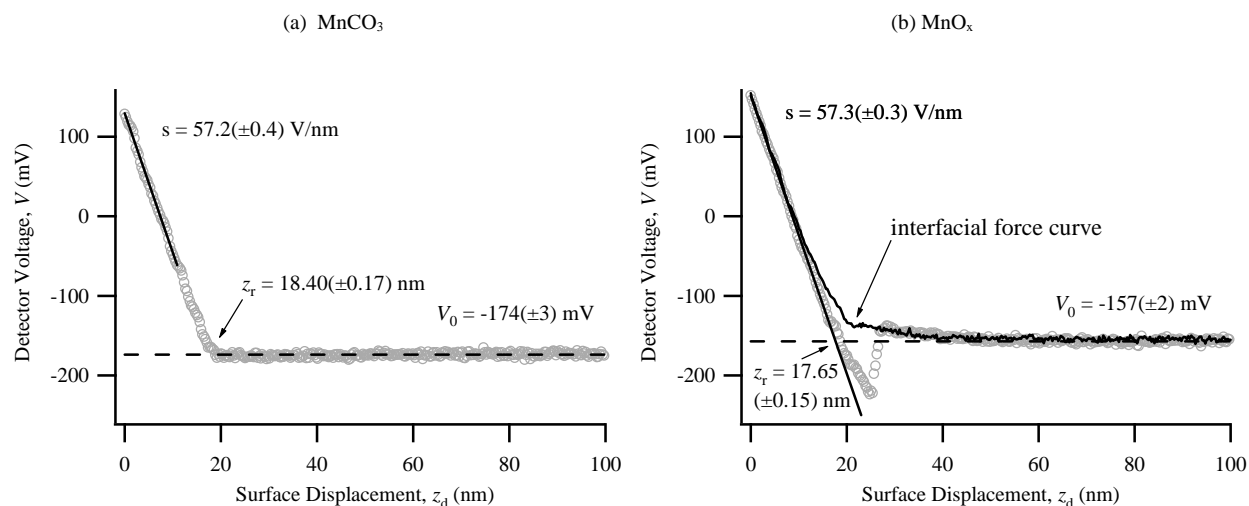


Figure S2. Raw data corresponding to the force-distance curves shown in Figure 1. Detector sensitivity s is similar for both the substrate and the nanostructures. The baseline voltage reading V_0 and the relaxed tip-reference distance of the surface z_r are obtained independently for the substrate and the nanostructures. The procedures used to estimate s , V_0 , and z_r are as follows. For the typical $V-z_d$ plot over the rhodochrosite substrate (e.g., Figure S2a) two regions can be identified, including the contact region where the probe tip is pressed against the surface and the noncontact region where they are separate. The contact region extends from z_d of 0 to ca. 18.40 nm, over which V increases proportionally to the decrease of z_d . The noncontact region spans from z_d of ca. 18.40 to 100 nm, over which V remains constant. The intersection of these two regions yields $z_r(\text{MnO}_x) = 18.40(\pm 0.17)$ nm. Detector sensitivity is estimated by performing a linear regression to the data in contact region. The slope of the linearity gives $s = 57.2(\pm 0.4)$ nm V^{-1} . Averaging V over the noncontact region gives $V_0(\text{MnO}_x) = -174(\pm 3)$ mV. We similarly obtain $s = 57.3(\pm 0.3)$ nm V^{-1} , $z_r = 17.65(\pm 0.15)$ nm, and $V_0 = -157(\pm 2)$ mV over the oxide nanostructure (Figure S2b).

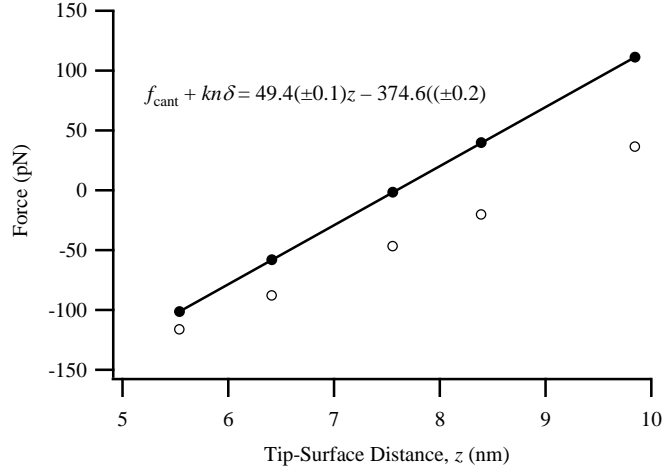


Figure S3. Linear regression of the transition data in Figure 1b. The original data are represented by open circles, and they are represented by the closed circles after being adjusted for stage movement. The logic for the adjustment is as follows. At the beginning of the transition regime where the cantilever and surface forces are still in balance, $f_{\text{cant}} = f_{\text{surf}} = -f_{\text{adh}}$ ($f_{\text{adh}} > 0$ and $f_{\text{surf}} = f_{\text{vdw}} + f_e < 0$). The minus signs indicate that f_{cant} has the opposite direction of action compared to f_{surf} and f_{adh} . As the surface moves downward into the transition regime for the n th step with a distance of δ (i.e., $\Delta z_d = n\delta$), the cantilever force becomes $f_{\text{cant}}(\Delta z_d) = -f_{\text{adh}} - k\Delta d$ ($\Delta d \leq 0$ due to the relaxation of the cantilever deflection). Since $z = z_d - z_r - d$ and z_r is constant (cf. Figure S1), $\Delta z = \Delta z_d - \Delta d$. Combining the above two results gives $f_{\text{cant}}(\Delta z_d) = -f_{\text{adh}} - k(\Delta z_d - \Delta z)$, which can be rearranged to $f_{\text{cant}}(\Delta z_d) + k\Delta z_d = -f_{\text{adh}} + k\Delta z$. Replacing Δz_d by $n\delta$ and $\Delta z = z - z_{\text{adh}}$, we now have a linear relation between $f_{\text{cant}}(\Delta z_d) + kn\delta$ and z : $f_{\text{cant}}(\Delta z_d) + kn\delta = kz - (f_{\text{adh}} + kz_{\text{adh}})$. The dependent term $f_{\text{cant}}(\Delta z_d) + kn\delta$ is the stage-movement adjusted cantilever force represented by the open circles with $n = 1, 2, 3, 4,$ and 5 and $\delta = 0.30$ nm. Linear regression of $f_{\text{cant}}(\Delta z_d) + kn\delta$ and z gives a slope of $49.4(\pm 0.1)$ pN nm $^{-1}$ and an intercept of $-374.6(\pm 0.2)$ pN, which agree well with $k = 48.8$ pN nm $^{-1}$ and $-(f_{\text{adh}} + kz_{\text{adh}}) = -(188 + 48.8 \times 3.0)$ pN = -334.4 pN. To further derive a criterion for the cantilever force to be in balance with surface forces, we can start with $f_{\text{cant}}(\Delta z_d) = -f_{\text{surf}}(\Delta z_d)$. Since $f_{\text{surf}}(\Delta z_d) = -f_{\text{adh}} + (df_{\text{surf}}/dz)\Delta z$ ($df_{\text{surf}}/dz > 0$ as shown in Figure 1b), replacing $f_{\text{cant}}(\Delta z_d)$ with $-f_{\text{adh}} - k\Delta d$ gives $k = -(df_{\text{surf}}/dz)\Delta z/\Delta d$. Replacing Δz with $\Delta z_d - \Delta d$ gives $k = (df_{\text{surf}}/dz)(1 - \Delta z_d/\Delta d)$. Since $\Delta z_d > 0$ and $\Delta d \leq 0$, this result indicates that $k \geq (df_{\text{surf}}/dz)$ is the criterion for tracking surface forces by the cantilever in force balance.

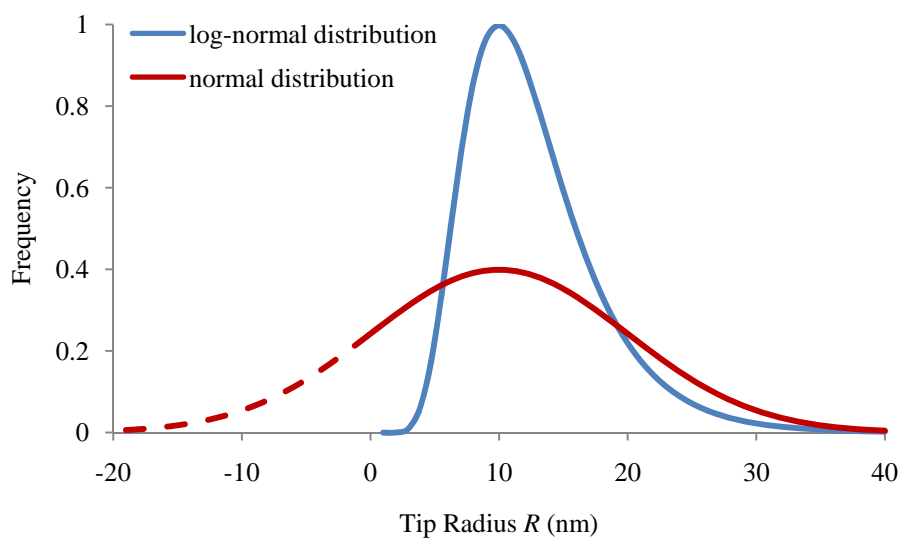


Figure S4. Uncertainty of the AFM tip radius.

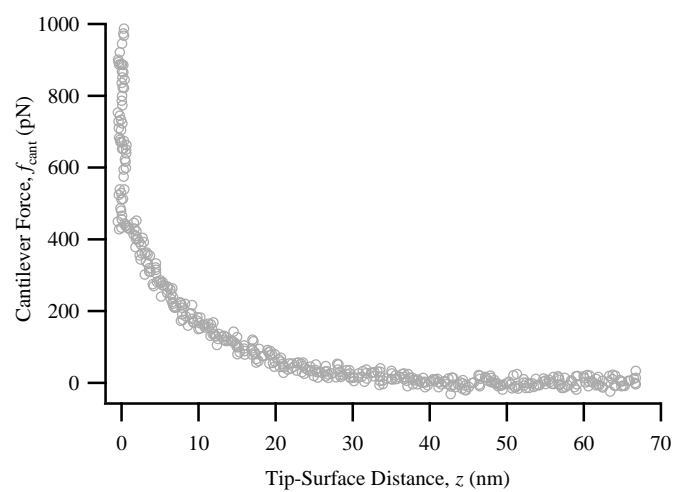


Figure S5. A representative force-distance curve showing that electrostatic repulsion dominates over van-der-Waals attraction. This result explains the negative $f_{\text{adh}}(\text{MnO}_x)$ values for the blue regions in Figure 2b.

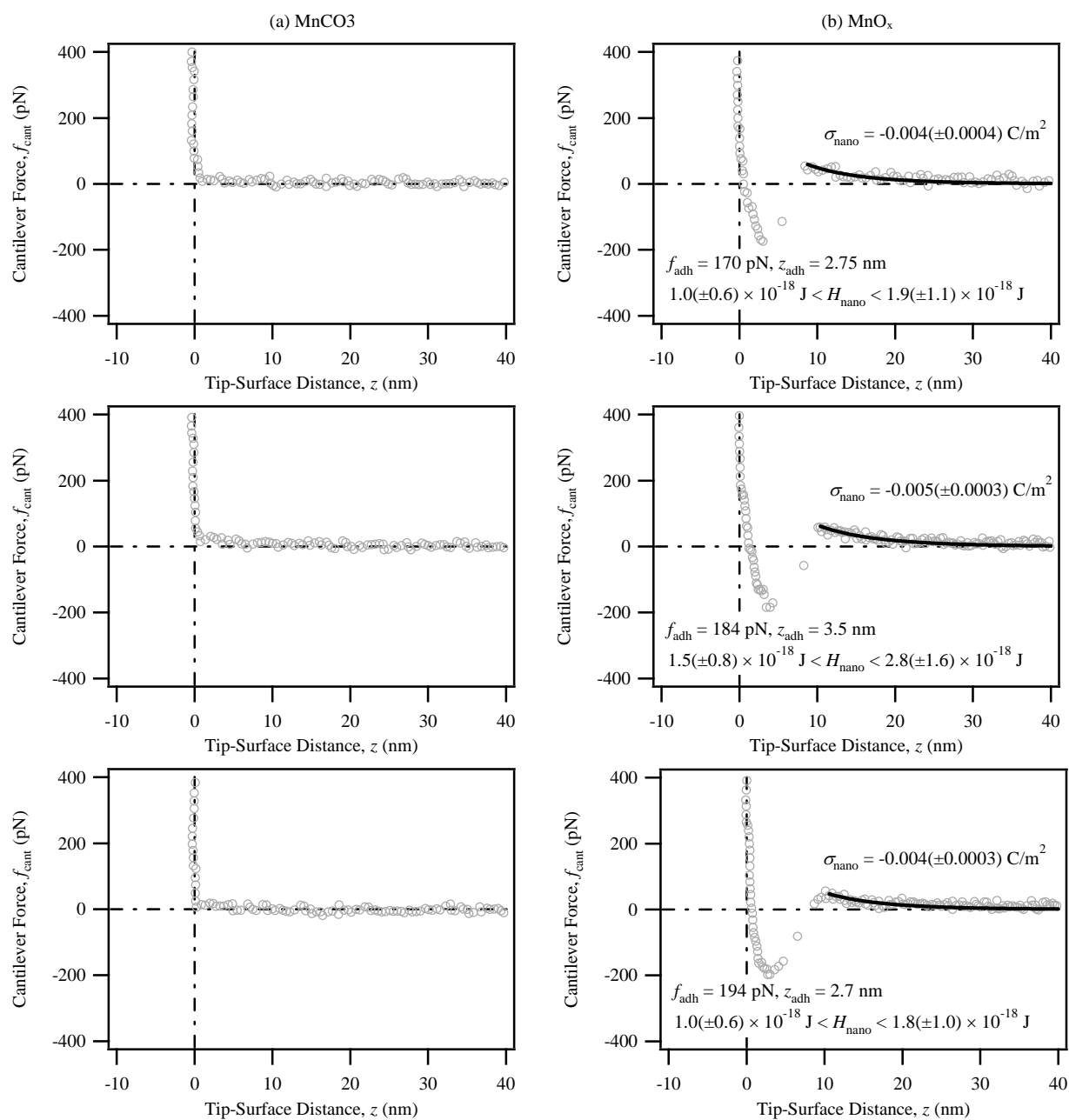


Figure S6. Three sets of representative force curves for (a) MnCO_3 and (b) MnO_x at pH 9.7 and with an ionic strength of 1 mM. See text for discussions related to the uncertainties of the estimates of σ_{nano} and H_{nano} .

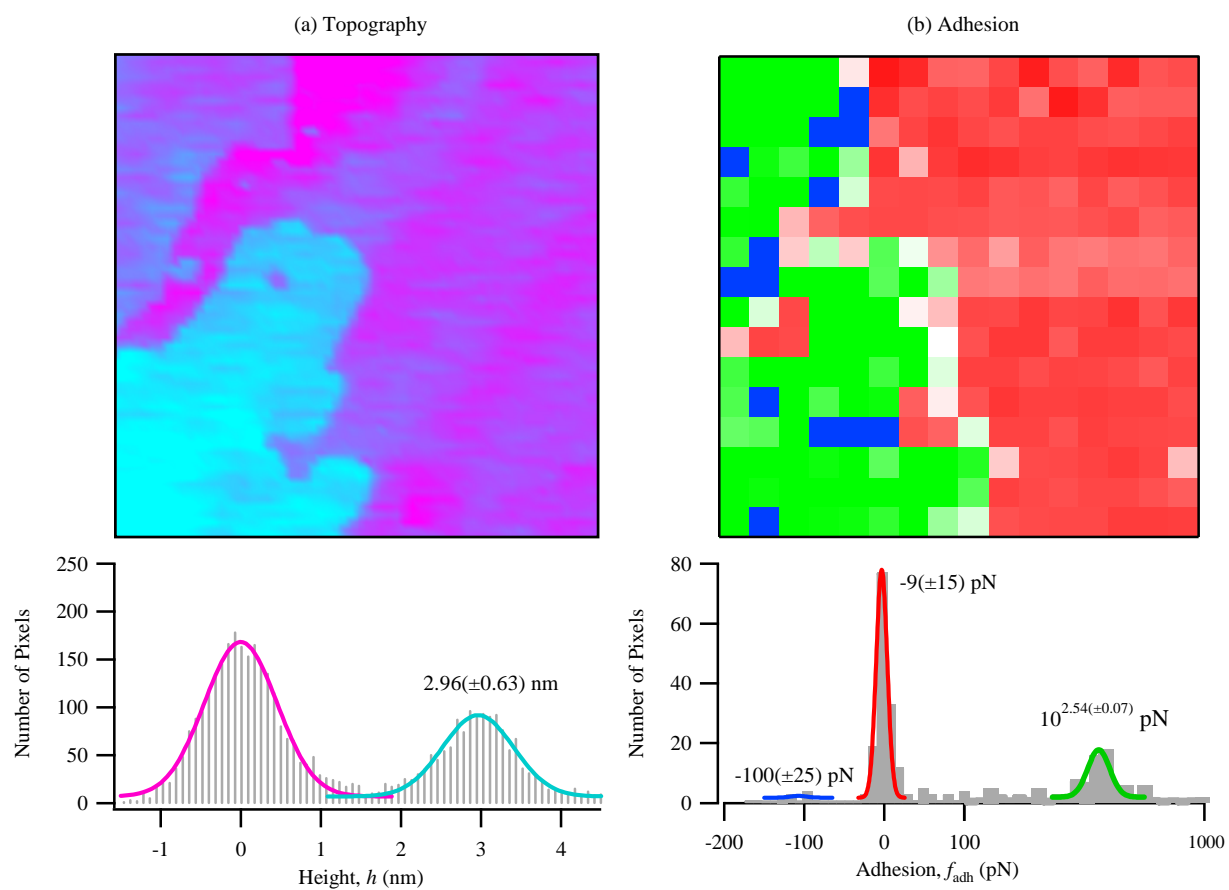


Figure S7. One set of topography and adhesion images at pH 9.5.